Topics in Catalysis
https://doi.org/10.1007/s11244-018-1072-5

ORIGINAL ARTICLE

Notable Reactivity of Acetonitrile Towards Li_2O_2/LiO_2 Probed by NAP XPS During Li–O_2 Battery Discharge

Tatiana K. Zakharchenko[1] · Alina I. Belova[1] · Alexander S. Frolov[1] · Olesya O. Kapitanova[1] · Juan-Jesus Velasco-Velez[2] · Axel Knop-Gericke[2,5] · Denis Vyalikh[3,4] · Daniil M. Itkis[1] · Lada V. Yashina[1]

Abstract
One of the key factors responsible for the poor cycleability of Li–O_2 batteries is a formation of byproducts from irreversible reactions between electrolyte and discharge product Li_2O_2 and/or intermediate LiO_2. Among many solvents that are used as electrolyte component for Li–O_2 batteries, acetonitrile (MeCN) is believed to be relatively stable towards oxidation. Using near ambient pressure X-ray photoemission spectroscopy (NAP XPS), we characterized the reactivity of MeCN in the Li–O_2 battery. For this purpose, we designed the model electrochemical cell assembled with solid electrolyte. We discharged it first in O_2 and then exposed to MeCN vapor. Further, the discharge was carried out in O_2 + MeCN mixture. We have demonstrated that being in contact with Li–O_2 discharge products, MeCN oxidizes. This yields species that are weakly bonded to the surface and can be easily desorbed. That's why they cannot be detected by the conventional XPS. Our results suggest that the respective chemical process most probably does not give rise to electrode passivation but can decrease considerably the Coulombic efficiency of the battery.

Keywords Li–O_2 battery · In situ NAP XPS · Acetonitrile · Side reactions

1 Introduction

Li–O_2 batteries promise extraordinary high specific energy that makes them interesting for the next generation power technologies [1, 2]. Unfortunately, at the moment many obstacles hinder the development and practical application of such type of batteries [3, 4]. One of such issues is poor cycle life associated with side reactions that involve the major discharge product lithium peroxide (Li_2O_2) and/or discharge intermediate lithium superoxide (LiO_2), electrode materials [5–7] and electrolytes [8, 9]. As a result of side reactions, Coulombic efficiency of the battery drops down, and electrode surface is passivated by side products. Currently many research efforts are focused at studying the chemical stability of electrolyte components—both solvents and salts—under Li–O_2 battery operation conditions [10–12]. Reactions of the electrolytes with commercially available and synthesized in-house Li_2O_2 [13, 14] and KO_2 [15], which is used instead of unstable LiO_2 [16], are also often investigated. Several publications report the theoretical simulations of electrolyte reactivity towards oxidation in Li–air batteries [17–19]. It was found that most of solvents that have ever been used as Li–O_2 battery electrolyte's

Electronic supplementary material The online version of this article (https://doi.org/10.1007/s11244-018-1072-5) contains supplementary material, which is available to authorized users.

✉ Lada V. Yashina
yashina@inorg.chem.msu.ru

[1] Lomonosov Moscow State University, Leninskie gory, Moscow, Russia 119991

[2] Depatment of Inorganic Chemistry, Fritz-Haber-Institut der Max-Planck-Gesellschaft, Faradayweg 4-6, 1495 Berlin, Germany

[3] IKERBASQUE, Basque Foundation for Science, 48011 Bilbao, Spain

[4] Departamento de Fisica de Materiales and CFM-MPC UPV/EHU, Donostia International Physics Center (DIPC), 20080 San Sebastian, Spain

[5] Department of Heterogeneous Reactions, Max-Planck-Institute for Chemical Energy Conversion, Stiftstraße 34,36, 45413 Mülheim, Germany

Published online: 25 October 2018

component—alkyl carbonates [20, 21], ethers [22, 23], amides [24, 25], dimethylsulfoxide (DMSO) [14, 26]—are to a different extent unstable towards oxidation by LiO_2 or/and Li_2O_2. At the same time, acetonitrile (MeCN) is considered to be among relatively stable solvents [8].

The commonly acknowledged reaction pathway of the electrolyte solvent degradation includes proton abstraction of α-CH_2 group by strong nucleophile—superoxide anion (O_2^-). It leads to oxidation [25] and, in addition, to polymerization [23] of the solvent molecules. Therefore, solvent tendency to oxidize is characterized by C–H dissociation constant pK_a, with the most stable molecules having the highest pK_a [19, 27]. Khetan et al. also show that pK_a value characterizes H-abstraction from solvent molecule at Li_2O_2 surface [28]. Due to the low pK_a value MeCN might be unstable to some extent towards oxidation by LiO_2 and Li_2O_2.

Value of pK_a is not, however, the only factor comprehensively describing the reactivity of the solvent with strong nucleophiles. Various functional groups can be also attacked by superoxide species. For instance, in case of DMSO O_2^- attacks −S=O group thus yielding –SO_2 [24]. As for MeCN, it is well-known that along with other nitriles of R-CN type it reacts with peroxide and superoxide anions in alkaline solutions yielding the corresponding amides $RCONH_2$ [29]. It was also found that MeCN can undergo self-condensation in contact with KO_2 containing KOH impurities, which results in 3-aminocrotonitrile [18]. Based on these data one can suppose MeCN can reveal certain reactivity towards both peroxides and superoxide in aprotic media also.

Unfortunately, it is difficult to experimentally trace possible chemical reactions of MeCN in Li–O_2 battery. First reason is that metallic Li anode reacts with MeCN forming lithium cyanide and, therefore, Li–O_2 test cells should either comprise a solid electrolyte membrane, which isolates lithium electrode [30, 31], or employ another counter electrode [32]. In addition, MeCN cannot be used as electrolyte for Li–air battery opened to the atmosphere because of its high volatility [19]. For these reasons, few works only have been devoted to the evaluation of MeCN chemical stability in Li–O_2 batteries up to now. In some reports, ex situ X-ray photoelectron spectroscopy (XPS) showed that MeCN is stable both in contact with Li_2O_2 [33] and under Li–O_2 battery operation conditions [10]. It is also supported by cyclic voltammetry results [19]. Theoretical modelling also predicts negligible reactivity and strong molecular adsorption of solvent at Li_2O_2 (1 0 $\bar{1}$ 0) surface [34]. All in all, the data reported earlier imply that acetonitrile solutions are considered to be a good choice for Li–O_2 batteries. Nevertheless, the data obtained by ex situ XPS often include certain artifacts related to surface contaminations and sample transfer. Direct in situ observations of products that can be formed during Li–O_2 battery discharge in presence of MeCN are currently missing.

Here we employ near ambient pressure X-ray photoelectron spectroscopy (NAP XPS) to characterize MeCN behavior in Li–O_2 battery. We designed a model electrochemical cell containing graphene electrode and Li-conductive solid electrolyte, while MeCN vapor was introduced in the gas phase. To trace the MeCN reactivity towards Li_2O_2 in situ we discharged the cell in O_2 followed by exposure to MeCN vapor. To evaluate possible reactions of MeCN with LiO_2 the discharge was continued in O_2 + MeCN mixture. We have demonstrated that in both cases MeCN is oxidized. This yields species that are weakly bonded to the surface and can be easily desorbed. That is why they cannot be detected by conventional ex situ XPS of clean Li_2O_2 and KO_2 surfaces exposed to MeCN vapors. Our results suggest that the respective chemical process probably does not give rise to electrode passivation but can decrease considerably the Coulombic efficiency of the battery.

2 Experimental

2.1 Preparation of Li_2O_2 and KO_2 Layers and Their Exposure to MeCN Vapor

Thin layers of Li_2O_2 and KO_2 free from contaminations were prepared by deposition of metallic Li or K on clean graphene substrate under oxygen (99.995% purity, Air liquid) pressure of 8×10^{-5} mbar in the preliminary baked preparation chamber of photoelectron spectrometer (base pressure $1–2\times10^{-9}$ mbar) at Russian-German beamline at BESSY II (Hemholtz Zentrum Berlin). As a substrate, we used commercial single layer graphene on Cu foil (Donghuk University, South Korea) grown by CVD [35]. It was preliminary heated at 600 °C for 40 min to obtain clean surface; the cleanness was confirmed by the absence of O 1*s* signal in XPS and by the typical shape of C-*K* edge NEXAFS spectra. Layers were deposited from Li or K dispensers (SAES). The absence of carbon contaminations from the Li and K source was preliminary checked by the deposition of same films on a clean WO_3 surface and further recording C 1*s* spectra.

Further Li_2O_2 and KO_2 layers were exposed to MeCN vapor with pressure of 1 mbar for 30 min. For this a vacuum-compatible flask was filled with MeCN (anhydrous, 99.8%, Sigma-Aldrich) in an Ar-filled glovebox (M. Braun). The flask was attached to the preparation chamber without exposure to air. The solvent in the flask was degassed by several freezing and evacuation cycles and then dosed to the chamber through a leak valve.

C 1*s*, O 1*s*, N 1*s* and Li 1*s* core level spectra of the clean graphene, Li_2O_2 and KO_2 films before and after their exposure to MeCN were acquired using a SPECS Phoibos 150

electron energy analyzer at a photoelectron kinetic energy of 200 eV. Photon energy was calibrated using 2nd order reflection of the plane grating. All spectra were fitted by Gaussian/Lorentzian convolution functions using Unifit 2014 software. Spectral background was optimized using a combination of Shirley and Tougaard functions simultaneously with spectral fitting.

2.2 Photoemission Study of the All-Solid-State Li–O_2 Cells

Electrochemical cell for in situ XPS studies is shown in Fig. S1. It had a sandwiched structure with graphene working electrode, Li-conductive solid electrolyte and metallic Li counter electrode. Graphene was transferred from Cu foil onto a solid glass–ceramic NASICON-type electrolyte ($Li_{1.5}Al_{0.5}Ge_{1.5}(PO_4)_3$) plate prepared in-house [36]. PMMA-based graphene transfer technique described elsewhere [37] was used. The transfer procedure was performed twice to get double-layer graphene on solid electrolyte surface. Such double-layer graphene possesses sufficient electron conductivity and is thin enough to provide laterally uniform transport of Li ions from solid electrolyte to the surface. After transfer electrode surface was cleaned from PMMA residues by washing in glacial acetic acid for 8 h.

The cells were assembled in an Ar-filled glovebox (M. Braun) by stacking the graphene/solid electrolyte plate and metallic lithium foil [5, 6]. After assembly the cells were transferred to the NAP XPS spectrometer of the ISISS beamline (HZB). The cells were discharged at either 1 mbar oxygen or 2 mbar MeCN + O_2 mixture (1:1 vol.). The discharge was carried out by applying constant current of 50 nA for various time periods. All electrochemical measurements were performed using SP-200 potentiostat/galvanostat (Bio-Logic SAS Instruments).

Photoemission spectra for the graphene electrode surface were measured both during discharge and at open circuit after certain discharge periods. C 1*s*, O 1*s*, N 1*s* and Li 1*s* core level spectra were acquired at a photoelectron kinetic energy of 200 eV using a SPECS Phoibos 150 NAP electron energy analyzer. The spectra were treated as described above.

2.3 DFT Modelling

Modelling of the MeCN + LiO_2 and MeCN + Li_2O_2 reaction paths, i.e. saddle points and local minima, was performed within density functional theory (DFT) using the B3LYP hybrid functional and the 6-311G basis set. Geometry optimization at local minimum points was carried out using the Berny algorithm, and at saddle points we applied the quadratic synchronous transit algorithm QST-2. Barriers were calculated within the framework of the transition state theory. To verify the transition state, a frequency analysis was performed. The variation of chemical shifts in XP-spectra are calculated as a difference in electrostatic potential at centre of each atom of interest between reagent and reaction product [38].

3 Results and Discussion

Earlier XPS studies of the commercial Li_2O_2 powder washed by MeCN revealed that unmodified MeCN molecules only adsorb at the surface [33], which allowed authors to suppose negligible reactivity of MeCN towards Li_2O_2. However, the reactivity of solid Li_2O_2 can be suppressed by common surface contaminations, such as adventitious carbon, Li_2CO_3 etc., observed in these experiments. In our experiments, we tried to provide cleaner conditions for the reactivity studies, i.e. we studied Li_2O_2 surface freshly prepared by Li deposition under pure oxygen in spectroscopically clean chamber. O 1*s* spectrum measured right after the deposition is presented in Fig. 1a. The deposited layer is mostly Li_2O_2 (531.5 eV) with minor O 1*s* intensity related to lithium oxide (528.8 eV) [39]. Varying photon energy and the corresponding electron kinetic energy from 200 to 50 eV we found that peroxide is located at the surface fully covering oxide (IMFP for Li_2O_2 at 200 eV is 9.2 Å and at 50 eV is 6.4 Å; details of calculation are given in Supplementary material file). It should be mentioned that we observe no static charging effect despite the poor electrical conductivity of Li_2O_2. We believe that no charging occurs as we prepare relatively thin layer of the deposit on well conductive substrate. Therefore, precise and reliable interpretation of spectral features becomes possible. After exposure of the sample to MeCN vapors for 30 min followed by evacuation and spectra recording in UHV chamber, nitrogen was observed at the surface. N 1*s* spectrum in Fig. 1c can be treated as a single component positioned at 399.4 eV and can be assigned to the adsorbed MeCN molecules [40]. The estimated thickness of the adsorbed layer is nearly to 1 monolayer. Since the surface is covered with MeCN molecules solely we can suppose that it does not react with fresh surface of Li_2O_2 surface that is in line with previously reported results [33]. No remarkable decrease of Li_2O_2 layer thickness estimated from the corresponding spectra quantification was observed additionally supporting no noticeable reactivity between MeCN and Li_2O_2.

We further probed the reactivity of MeCN with superoxide species. Since LiO_2 is unstable at room temperature we made further experiments with freshly prepared KO_2 layer. After deposition of K in oxygen atmosphere the layer containing considerable amount of KO_2 was obtained. The corresponding binding energy in O 1*s* spectrum in Fig. 1b is 533.8 eV. Other spectral features are

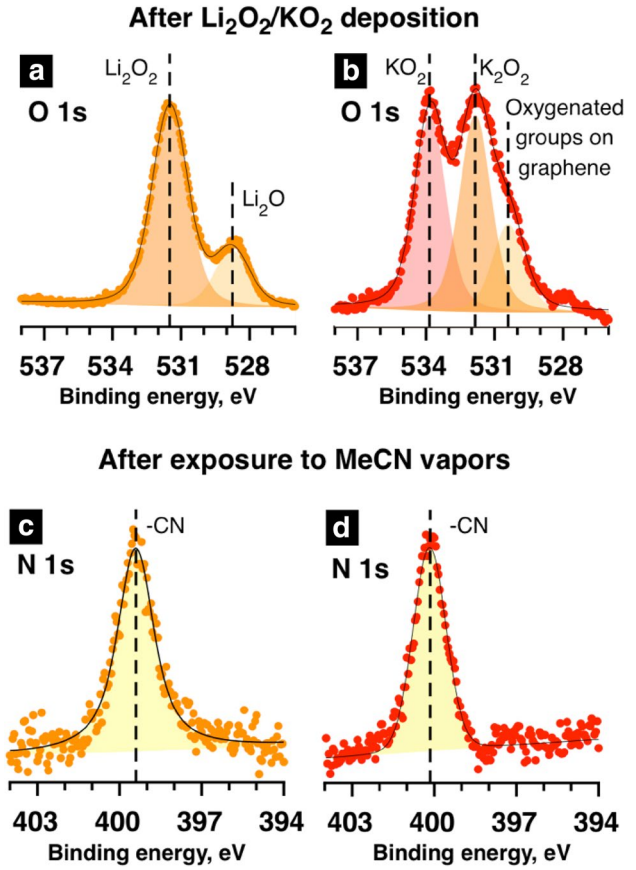

Fig. 1 O 1*s* photoemission spectra of graphene surface ($h\nu = 727$ eV, KE = 200 eV) after the deposition of Li (**a**) and K (**b**) at $P(O_2) = 8 \times 10^{-5}$ mbar evidencing Li_2O_2 and KO_2 formation correspondingly. N 1*s* spectra ($h\nu = 600$ eV, KE = 200 eV) after exposure to MeCN for Li_2O_2 (**c**) and for KO_2 (**d**) vapor ($P = 1$ mbar)

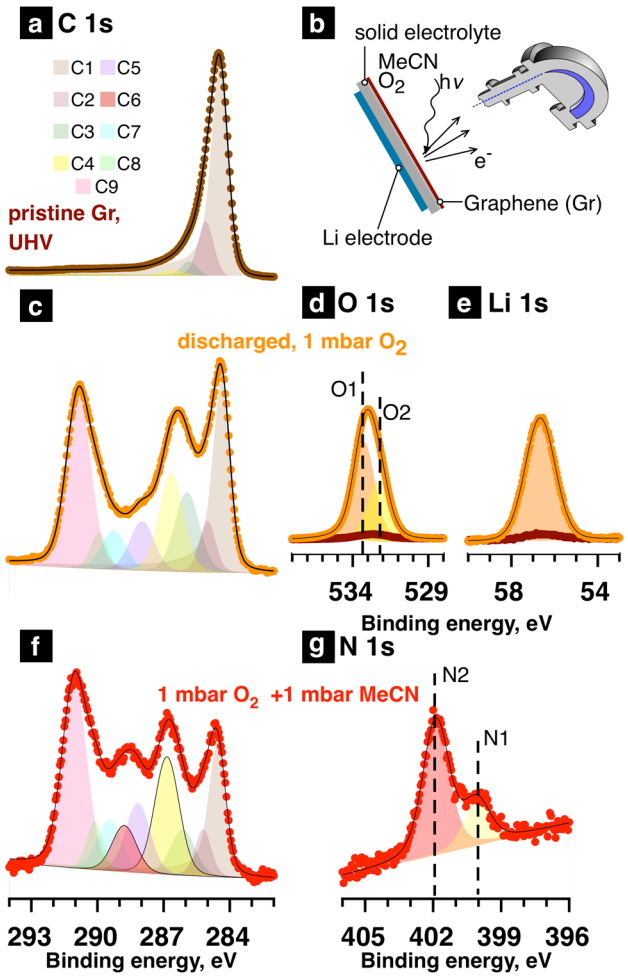

Fig. 2 C 1*s* spectra of pristine graphene electrode surface obtained at $h\nu = 485$ eV (**a**), after galvanostatic discharge in 1 mbar O_2 (**c**); after exposure to 1 mbar of MeCN (**f**); **b** schematic representation of electrochemical cell for in situ NAP XPS studies; O 1*s* (**d**), $h\nu = 727$ eV (O1 component relates to oxygenated groups on graphene, O_2 to Li_2O_2) and Li 1*s*, $h\nu = 256$ eV (**e**) before and after cell discharge under 1 mbar O_2. **g** N 1*s* spectra after exposition of discharge products to MeCN vapor, $h\nu = 600$ eV

related to potassium peroxide and products of the known reaction between KO_2 and graphene [39]. After exposure of the sample to MeCN vapor and further evacuation we found nitrogen at the surface, with N 1*s* being positioned at 400.2 eV.

We assigned this peak to acetonitrile molecularly adsorbed at the surface despite of the notable difference in its position with MeCN on Li_2O_2 as nitrogen chemical shift under monolayer coverage depends remarkably on the substrate nature [41]. The tendency of MeCN to be adsorbed molecularly at Li_2O_2 is in line with previous calculations [34]. Although we did not observe significantly oxidized nitrogen after its contact with KO_2, superoxide was considerably consumed during the exposure in contrast to Li_2O_2 (Fig. S2), but it can also arise from its general instability, as we observed in additional experiments.

As lithium superoxide may be much more reactive than KO_2, we further performed in situ studies of Li–O_2 cell to enable correct evaluation of the MeCN reactivity towards Li_2O_2 and LiO_2.

For in situ NAP XPS studies we used electrochemical cell with solid electrolyte and graphene electrode, which is schematically shown in Fig. 2b. Graphene is suggested as the thinnest imaginable electrode, which possesses a high electronic conductivity and good mechanical properties. Moreover, its flat morphology provides effective ionic contact between the graphene and polished glass–ceramic electrolyte. C 1*s* spectrum for pristine graphene electrode is shown on Fig. 3a. It can be fitted with the dominating intensity of sp^2 carbon (marked as C1) and certain contribution of β-sp^2 (C2). Besides one can see unessential surface contamination by oxygenated groups (C3 and C4).

To probe MeCN reactivity with Li–O_2 battery discharge product Li_2O_2 (or other possible products) we firstly

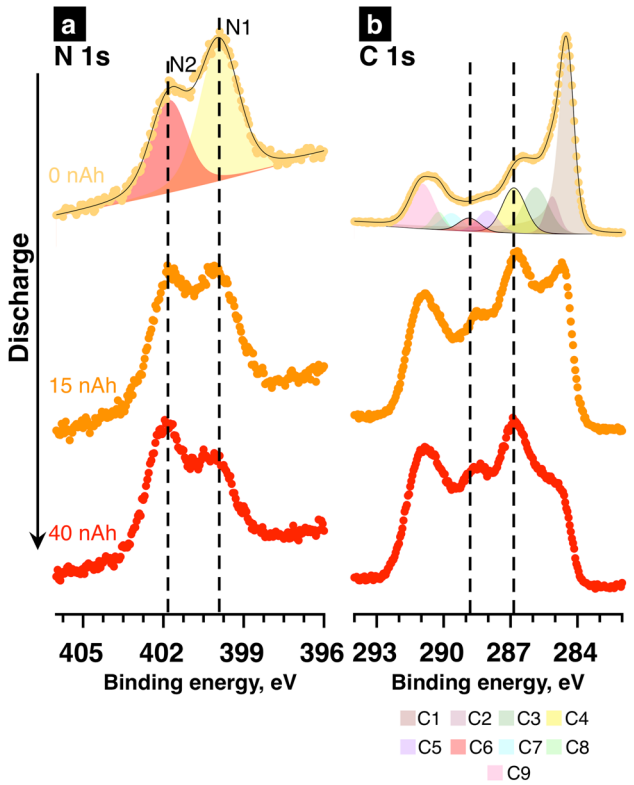

Fig. 3 Evolution of N 1*s* (**a**) and C 1*s* (**b**) spectra for graphene cathode during Li–O_2 cell discharge in O_2 + MeCN gas mixture (1:1), total pressure 2 mbar

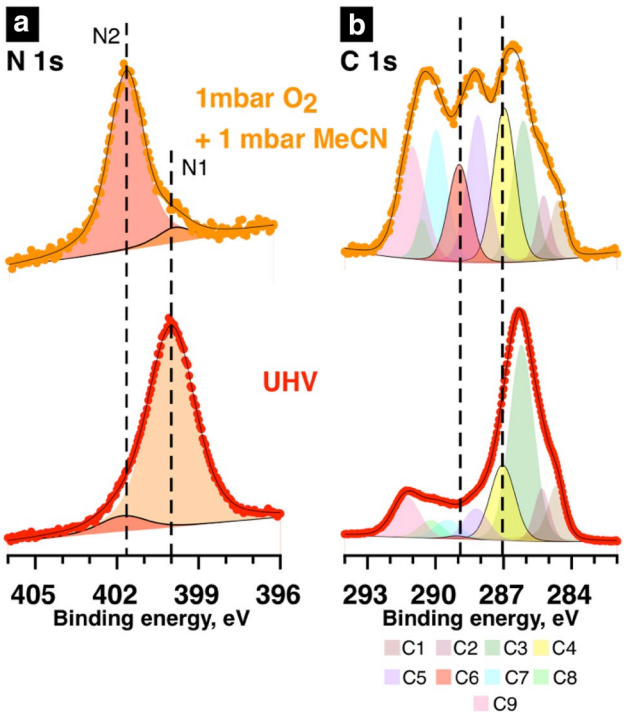

Fig. 4 N 1*s* (**a**) and C 1*s* (**b**) spectra of graphene cathode after Li–O_2 cell discharge recorded in O_2 + MeCN gas mixture (1:1) of total pressure 2 mbar (top) and in UHV conditions (bottom)

discharged the cell in pure oxygen and further exposed it to MeCN + O_2 gas mixture. Upon the discharge the surface concentration of lithium and oxygen significantly increased as it follows from O 1*s* and Li 1*s* spectra presented in Fig. 2d, e, correspondingly. During discharge LiO_2 reacts with graphene and is spent rapidly generating a number of oxygen-containing species (C3–C8) including lithium carbonate (C8) [5]. According to O 1*s* spectrum in Fig. 2d no LiO_2 remains just before MeCN exposure. After introducing MeCN vapors in the analysis chamber nitrogen appears at the surface. N 1*s* spectrum in Fig. 2g measured in the gas mixture has two components positioned at binding energy of 401.9 eV (component N2) and 400.05 eV (component N1). N1 is related to MeCN [41], whereas the spectral feature N2 corresponds to the higher positive charge at nitrogen atoms in reaction products. In C 1*s* spectrum in Fig. 2f new intense component appeared at binding energy of 288.8 eV that also have binding energy higher than that of pure MeCN also evidencing for the formation of some byproducts at the surface.

Afterwards, to evaluate possible reactions of MeCN with intermediates such as LiO_2 [5] we further discharged the cell under MeCN + O_2 vapor. During discharge LiO_2 is generated in the presence of MeCN. Again, we observed two coexisting peaks in N 1*s* spectra—one for MeCN (component N1) and another for its oxidation product (component N2), which is illustrated in Fig. 3a. At the same time, the spectral features C4 at 287.0 eV and C6 at 288.8 eV in C 1*s* spectra in Fig. 3b increased upon discharge. We ascribe these peaks to MeCN and its oxidation product, correspondingly. The chemical nature of the product is the same as for Li_2O_2.

All in all, observation of new spectral features in both N 1*s* and C 1*s* makes us to believe that MeCN demonstrates certain reactivity towards Li–O_2 cell discharge product Li_2O_2. The resulting side products can be detected, however, exclusively in presence of MeCN vapors during spectral acquisition. Alternatively, the presence of oxygen in the spectroelectrochemical experiments may be the reason why we do not see the reaction products in the ex situ experiments. Nevertheless, after chamber evacuation to pressure lower than 10^{-7} mbar the oxidation product desorbs as it clearly follows from spectra in Fig. 4, which illustrates the spectral changes upon evacuation of the cell after discharge in MeCN + O_2 gas mixture. Under UHV conditions the major N 1*s* signal goes from MeCN (N1, 400 eV). This indicates stronger MeCN adsorption at Li_2O_2 surface in comparison with its oxidation product. For this reason, we observed molecularly adsorbed MeCN rather than reaction products at Li_2O_2 surface in our ex situ experiments described above. At the same time no significant loss of Li_2O_2 after the exposure

evidences low rate of the MeCN conversion under conditions applied.

As the electrode surface is covered by carbon oxidation species they may also react with acetonitrile. However, the comparison of data obtained for cell with rather different concentration of these species allows us to conclude that MeCN does react with Li_2O_2. Spectra for this cell are shown in Fig. S4.

Notable reactivity of MeCN may have two consequences: (i) the electrode surface is most probably not passivated by this side reaction product, although this also depends on the product solubility in liquid MeCN (ii) Columbic efficiency can drop essentially if this reaction is fast enough since Li_2O_2 is spent during this process. Fortunately, at least under conditions of our ex situ experiments, the conversion rate is not high, and acetonitrile-based electrolytes are considered as promising aprotic media for oxygen reduction.

Now we are discussing the reliability of the above reported observations, as X-ray beam can essentially modify the sample [42], especially in case if oxygen is one of the components of gas mixture. To evaluate the contribution of possible beam effect during cell discharge in gas mixture we registered the spectra at three different points of our electrode with different X-ray exposure time (Fig. S3). We found no correlation between N1 and N2 component intensities ratio and beam exposure time. Contrary, there is strong correlation between the N2/N1 ratio and the charge passed through the electrochemical cell. This imply that the appearance of N2 component in N 1*s* spectra is not due to the X-ray beam effect, supporting the hypothesis that MeCN does oxidize during battery discharge.

Summing up, after the discharge of Li–O_2 cell in the presence of MeCN vapor we observed two features in N 1*s* photoemission spectrum positioned at 400 eV (N2) and 401.8 eV (N1), and in C 1*s* spectrum 287 eV (C4) and 288.8 eV (C6). N2 and C4 are assigned to MeCN adsorbed at the surface. Typical binding energies for nitrogen-containing functional groups are collected in Table 1.

It is known that nitriles are oxidized to amides by H_2O_2 in the presence of strong base (usually OH^-) [29]. Component C6 in C 1*s* spectra can be related to amide group, but N 1*s* binding energy for amide is close to initial MeCN − 400 eV. Therefore, amide group is probably present in the oxidation products but does not explain the appearance of N1 component. Typically, the binding energy value of 401.8 eV is associated with quaternary amine or ammonia [47, 48]. However, the lack of available hydrogen atoms in our system (e.g., CH_3– group in MeCN), makes the transformation of –CN group to NH_4^+ rather unlikely. Typically, the binding energy for N–O bonds is in the range from 400 to 405.8 eV depending on compound [49–52], that fits well to our observations. However, the detailed knowledge of the oxidation products and reaction mechanism definitely needs additional study, for instance, via detailed in situ analysis of electrolyte composition.

Table 1 A summary of spectral features for various of nitrogen-containing functional groups

Component	Binding energy, eV		References
	C 1*s*	N 1*s*	
–CN	287.0	400.2	[41]
	286.6	399.9	[43]
–C(O)–NH_2	288.3	400	[44]
	287.4	400.1	[45]
	288.2	400.0	[46]
NH_3	–	400	[47]
NR_4^+	–	401.8	[48]
NH_4^+	–	401.8	[47]
–N=O	–	400 ± 0.5	[49]
	–	403.7	[50]
$–N^+–O^-$	–	402.5	[51]
$–NO_2$	–	405.8	[52]

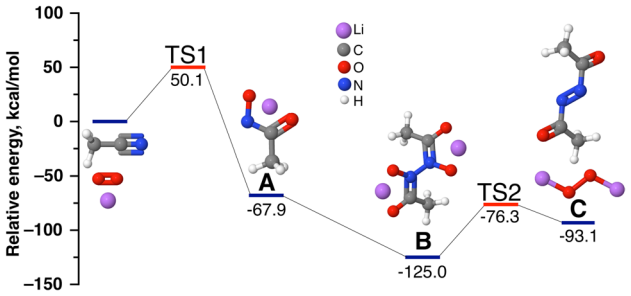

Fig. 5 Simulated reaction path for MeCN oxidation by LiO_2

To get further insight into MeCN reactivity and to get a hint on the nature of MeCN oxidation products we used DFT modelling for simplified system at a molecular level. In detail, LiO_2, Li_2O_2 and MeCN were considered as molecules in vacuum. The proposed reaction path is illustrated in Fig. 5 (the corresponding reaction scheme is shown in Fig. S5 of Supplementary material file). At the first step LiO_2 reacts with MeCN by free-radical addition mechanism forming the radical *A*. It contains unpaired electron on nitrogen sp^2 orbital. The second step is the dimerization of two *A* species by free-radical addition mechanism. As a result, dilithium diacetylhydrazine-1,2-bis(olate) molecule *B* forms. It contains N–N bond. We assume that the final product *C* (E)-diacetyldiazene is formed by monomolecular elimination of Li_2O_2 molecule.

The comparison of experimental and calculated chemical shifts in Table 2 supposes that we detect intermediate species *A* at the surface of discharge products in operando conditions. Final product evidently desorbs under UHV. This

Table 2 The experimental and calculated core level shifts for oxidation products with respect to MeCN (Figs. 5, 6)

	C 1*s*, eV	N 1*s*, eV
Experimental	1.8	1.8
Calculated		
A	1.70	1.06
B	1.94	3.24
C	2.95	2.86
D	0.43	-0.25
E	0.01	0.65

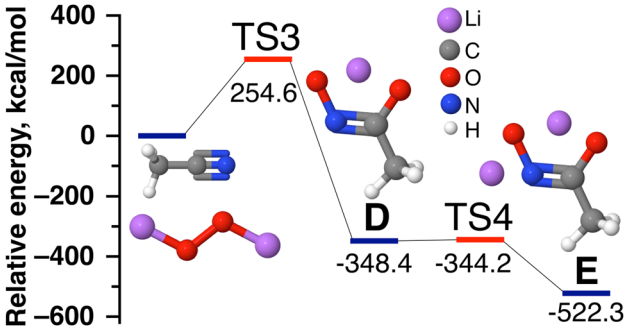

Fig. 6 Simulated reaction path for MeCN oxidation by Li_2O_2

is supported by the fact that the estimated vapor pressure of (E)-diacetyldiazene is 3.4 ± 0.4 mbar at RT [53].

According to the calculations acetonitrile oxidation by Li_2O_2 via similar route is unfavorable. We propose another reaction pathway illustrated in Fig. 6 (the corresponding reaction scheme is shown in Fig. S6 of Supplementary material file). Here the barrier (*TS3*) is still five times higher than for oxidation by LiO_2 (*TS1*). Product *D* turns out to be final oxidation product, with the further interaction with superoxide or peroxide molecules being hindered sterically. This makes dimerization (like transformation from *A* to *B*) impossible since there is no unpaired electron at the nitrogen atom. Product *D* can transform to its isomer *E* that has lower formation energy due to decrease of electrostatic interaction energy between two lithium cations. This is achieved by their spatial separation through the transfer of one of the lithium atoms closer to oxygen and nitrogen.

4 Conclusions

We elaborated the electrochemical cell, which contains the graphene electrode and Li-conductive solid electrolyte. Solvent vapor was admitted in the gas phase. We have studied the reactivity of MeCN, which is suggested to be one of the most stable aprotic media for oxygen reduction. To trace its reactivity towards Li_2O_2, we discharged the cell in O_2 followed by exposure to MeCN vapor, while to evaluate possible reactions of MeCN with LiO_2 the discharge was continued in O_2 + MeCN mixture.

We demonstrated that in both cases MeCN becomes oxidized yielding species that are weakly bonded to the surface and can be easily desorbed. It makes the detection of these species hardly possible by conventional ex situ XPS of clean Li_2O_2 and KO_2 surfaces exposed to MeCN vapors. However, it may considerably decrease the Coulombic efficiency of the battery if the oxidation reaction rate is high. Nevertheless, our ex situ data evidence indirectly that, fortunately, it is not the case.

Acknowledgements This work of A.K-G., J.J.V-V. and D.M.I. was supported by the Russian Ministry of Science and Education (RFMEFI61614×0007) and Bundesministerium für Bildung and Forschung (Project No. 05K2014) in the framework of the joint Russian-German research project "SYnchrotron and NEutron STudies for Energy Storage (SYNESTESia)". T.K.Z acknowledges Center for Electrochemical Energy of Skolkovo Institute of Science and Technology for financial support. The work of O.O.K., A.I.B and L.V.Y. is performed within the joint project of the Russian Science Foundation (16-42-01093) and DFG (LA655-17/1). We are grateful to HZB for beamtime granted at ISISS and RGBL beamlines. T.K.Z. and A.S.F. thank to the Russian German laboratory at HZB for support provided. Authors are appreciated to Victor Vizgalov for solid electrolyte membrane preparation. Travelling of T.K.Z. was supported by German-Russian Interdisciplinary Science Center (G-RISC).

References

1. Bruce PG, Freunberger SA, Hardwick LJ, Tarascon J-M (2011) Li–O_2 and Li–S batteries with high energy storage. Nat Mater 11:19–29
2. Christensen J, Albertus P, Sanchez-Carrera RS, Lohmann T, Kozinsky B, Liedtke R, Ahmed J, Kojic A (2012) A critical review of Li/Air batteries. J Electrochem Soc 159:R1–R30
3. Lu Y-C, Gallant BM, Kwabi DG, Harding JR, Mitchell RR, Whittingham MS, Shao-Horn Y (2013) Lithium–oxygen batteries: bridging mechanistic understanding and battery performance. Energy Environ Sci 6:750–768
4. Li Y, Wang X, Dong S, Chen X, Cui G (2016) Recent advances in non-aqueous electrolyte for rechargeable Li-O_2 batteries. Adv Energy Mater 6:1600751–1600726
5. Itkis DM, Semenenko DA, Kataev EY, Belova AI, Neudachina VS, Sirotina AP, Hävecker M, Teschner D, Knop-Gericke A, Dudin P, Barinov A, Goodilin EA, Shao-Horn Y, Yashina LV (2013) Reactivity of carbon in lithium–oxygen battery positive electrodes. Nano Lett 13:4697–4701
6. Kozmenkova AY, Kataev EY, Belova AI, Amati M, Gregoratti L, Velasco-Vélez J, Knop-Gericke A, Senkovsky B, Vyalikh DV, Itkis DM, Shao-Horn Y, Yashina LV (2016) Tuning surface chemistry of TiC electrodes for lithium–air batteries. Chem Mater 28:8248–8255
7. McCloskey BD, Speidel A, Scheffler R, Miller DC, Viswanathan V, Hummelshøj JS, Nørskov JK, Luntz AC (2012) Twin problems of interfacial carbonate formation in nonaqueous Li–O_2 batteries. J Phys Chem Lett 3:997–1001

8. Balaish M, Kraytsberg A, Ein-Eli Y (2014) A critical review on lithium-air battery electrolytes. Phys Chem Chem Phys 16:2801–2822
9. Sharon D, Hirshberg D, Afri M, Garsuch A, Frimer AA, Aurbach D (2015) Lithium-oxygen electrochemistry in non-aqueous solutions. Isr J Chem 55:508–520
10. Marchini F, Herrera S, Torres W, Tesio AY, Williams FJ, Calvo EJ (2015) Surface study of lithium–air battery oxygen cathodes in different solvent–electrolyte pairs. Langmuir 31:9236–9245
11. Veith GM, Nanda J, Delmau LH, Dudney NJ (2012) Influence of lithium salts on the discharge chemistry of Li–air cells. J Phys Chem Lett 3:1242–1247
12. Nasybulin E, Xu W, Engelhard MH, Nie Z, Burton SD, Cosimbescu L, Gross ME, Zhang J-G (2013) Effects of electrolyte salts on the performance of Li–O_2 batteries. J Phys Chem C 117:2635–2645
13. Chalasani D, Lucht BL (2012) Reactivity of electrolytes for lithium-oxygen batteries with Li_2O_2. ECS Electrochem Lett 1:A38–A42
14. Kwabi DG, Batcho TP, Amanchukwu CV, Ortiz-Vitoriano N, Hammond P, Thompson CV, Shao-Horn Y (2014) Chemical instability of dimethyl sulfoxide in lithium–air batteries. J Phys Chem Lett 5:2850–2856
15. Schwenke KU, Meini S, Wu X, Gasteiger HA, Piana M (2013) Stability of superoxide radicals in glyme solvents for non-aqueous Li–O_2 battery electrolytes. Phys Chem Chem Phys 15:11830–11839
16. Qiu SL, Lin CL, Chen J, Strongin M (1989) Photoemission studies of the interaction of Li and solid molecular oxygen. Phys Rev B 39:6194–6197
17. Chau VKC, Chen Z, Hu H, Chan K-Y (2016) Exploring solvent stability against nucleophilic attack by solvated LiO_2^- in an aprotic Li-O_2 battery. J Electrochem Soc 164:A284–A289
18. Bryantsev VS, Giordani V, Walker W, Blanco M, Zecevic S, Sasaki K, Uddin J, Addison D, Chase GV (2011) Predicting solvent stability in aprotic electrolyte Li-air batteries: nucleophilic substitution by the superoxide anion radical ($O_2^{\bullet-}$). J Phys Chem A 115:12399–12409
19. Bryantsev VS, Uddin J, Giordani V, Walker W, Addison D, Chase GV (2012) The identification of stable solvents for nonaqueous rechargeable Li-Air batteries. J Electrochem Soc 160:A160–A171
20. McCloskey BD, Bethune DS, Shelby RM, Girishkumar G, Luntz AC (2011) Solvents' critical role in nonaqueous lithium–oxygen battery electrochemistry. J Phys Chem Lett 2:1161–1166
21. Freunberger SA, Chen Y, Peng Z, Griffin JM, Hardwick LJ, Bardé F, Novák P, Bruce PG (2011) Reactions in the rechargeable lithium–O_2 battery with alkyl carbonate electrolytes. J Am Chem Soc 133:8040–8047
22. Leskes M, Moore AJ, Goward GR, Grey CP (2013) Monitoring the electrochemical processes in the lithium–air battery by solid state NMR spectroscopy. J Phys Chem C 117:26929–26939
23. Freunberger SA, Chen Y, Drewett NE, Hardwick LJ, Bardé F, Bruce PG (2011) The lithium-oxygen battery with ether-based electrolytes. Angew Chem Int Ed 50:8609–8613
24. Sharon D, Afri M, Noked M, Garsuch A, Frimer AA, Aurbach D (2013) Oxidation of dimethyl sulfoxide solutions by electrochemical reduction of oxygen. J Phys Chem Lett 4:3115–3119
25. Chen Y, Freunberger SA, Peng Z, Bardé F, Bruce PG (2012) Li–O_2 battery with a dimethylformamide electrolyte. J Am Chem Soc 134:7952–7957
26. Sharon D, Hirsberg D, Afri M, Garsuch A, Frimer AA, Aurbach D, Takami N (2014) Reactivity of amide based solutions in lithium–oxygen cells. J Phys Chem C 118:15207–15213
27. Frimer AA, Farkash-Solomon T, Aljadeff G (1986) Mechanism of the superoxide anion radical (O_2^-) mediated oxidation of diarylmethanes. J Org Chem 51:2093–2098
28. Khetan A, Pitsch H, Viswanathan V (2014) Solvent degradation in nonaqueous Li-O_2 batteries: oxidative stability versus H-abstraction. J Phys Chem Lett 5:2419–2424
29. Sawaki Y, Ogata Y (1981) Mechanism of the reaction of nitriles with alkaline hydrogen peroxide. Reactivity of peroxycarboximidic acid and application to superoxide ion reaction. Bull Chem Soc Jpn 54:793–799
30. Aleshin GY, Semenenko DA, Belova AI, Zakharchenko TK, Itkis DM, Goodilin EA, Tretyakov YD (2011) Protected anodes for lithium-air batteries. Solid State Ionics 184:62–64
31. Bergner BJ, Busche MR, Pinedo R, Berkes BB, Schröder D, Janek J (2016) How to improve capacity and cycling stability for next generation Li–O_2 batteries: approach with a solid electrolyte and elevated redox mediator concentrations. ACS Appl Mater Interfaces 8:7756–7765
32. Johnson L, Li C, Liu Z, Chen Y, Freunberger SA, Tarascon J-M, Praveen BB, Dholakia K, Bruce PG (2014) The role of LiO_2 solubility in O_2 reduction in aprotic solvents and its consequences for Li–O_2 batteries. Nat Chem 6:1091–1099
33. Younesi R, Norby P, Vegge T (2014) A new look at the stability of dimethyl sulfoxide and acetonitrile in Li-O_2 batteries. ECS Electrochem Lett 3:A15–A18
34. Laino T, Curioni A (2013) Chemical reactivity of aprotic electrolytes on a solid Li_2O_2 surface: screening solvents for Li–air batteries. New J Phys 15:095009
35. Gunes F, Han GH, Kim KK, Kim ES, Chae SJ (2009) Large-area graphene-based flexible transparent conducting films. Nano 04:83–90
36. Vizgalov V, Nestler T, Trusov LA, Bobrikov I, Ivankov OI, Avdeev M, Motylenko M, Brendler E, Vyalikh A, Mayer DC, Itkis DM (2018) Enhancing lithium-ion conductivity in NASICON glass-ceramics by adding yttria. CrystEngComm 20:1375–1382
37. Her M, Beams R, Novotny L (2013) Graphene transfer with reduced residue. Phys Lett A 377:1455–1458
38. Yashina LV, Zyubina TS, Püttner R, Zyubin AS, Shtanov VI, Tikhonov EV (2008) A combined photoelectron spectroscopy and ab initio study of the adsorbate system O_2/PbTe(001) and the oxide layer growth kinetics. J Phys Chem C 112:19995–20006
39. Kataev EY, Itkis DM, Fedorov AV, Senkovsky BV, Usachov DY, Verbitskiy NI, Grüneis A, Barinov A, Tsukanova DY, Volykhov AA, Mironovich KV, Krivchenko VA, Rybin MG, Obraztsova ED, Laubschat C, Vyalikh DV, Yashina LV (2015) Oxygen reduction by lithiated graphene and graphene-based materials. ACS Nano 9:320–326
40. Tao F, Chen XF, Wang ZH, Xu GQ (2002) Binding and structure of acetonitrile on Si(111)-7 × 7. J Phys Chem B 106:3890–3895
41. Tao F, Wang ZH, Qiao MH, Liu Q, Sim WS, Xu GQ (2001) Covalent attachment of acetonitrile on Si(100) through Si–C and Si–N linkages. J Chem Phys 115:8563–8569
42. Liu J, Roberts M, Younesi R, Dahbi M, Edström K, Gustafsson T, Zhu J (2013) Accelerated electrochemical decomposition of Li_2O_2 under X-ray illumination. J Phys Chem Lett 4:4045–4050
43. Oultache AK, Prud'homme RE (2000) XPS studies of Ni deposition on polymethyl methacrylate and poly (styrene-co-acrylonitrile). Polym Adv Technol 11:316–323
44. Olivares O, Likhanova NV, Gómez B, Navarrete J, Llanos-Serrano ME, Arce E, Hallen JM (2006) Electrochemical and XPS studies of decylamides of α-amino acids adsorption on carbon steel in acidic environment. Appl Surf Sci 252:2894–2909
45. Cecchet F, Pilling M, Hevesi L, Schergna S, Wong JKY, Clarkson GJ, Leigh DA, Rudolf P (2003) Grafting of benzylic amide macrocycles onto acid-terminated self-assembled monolayers studied by XPS, RAIRS, and contact angle measurements. J Phys Chem B 107:10863–10872

46. Fustin CA, Gouttebaron R, De Nadaı C, Caudano R (2001) Photoemission study of pristine and potassium intercalated benzylic amide [2] catenane films. Surf Sci 474:37–46
47. Sano T, Mera N, Kanai Y, Nishimoto C, Tsutsui S, Hirakawa T, Negishi N (2012) Origin of visible-light activity of N-doped TiO_2 photocatalyst: behaviors of N and S atoms in a wet N-doping process. Appl Catal B 128:77–83
48. Wielant J, Hauffman T, Blajiev O, Hausbrand R, Terryn H (2007) Influence of the iron oxide acid–base properties on the chemisorption of model epoxy compounds studied by XPS. J Phys Chem C 111:13177–13184
49. Batich CD, Donald DS (1984) X-ray photoelectron spectroscopy of nitroso compounds: relative ionicity of the closed and open forms. J Am Chem Soc 106:2758–2761
50. Beard BC (1990) Cellulose nitrate as a binding energy reference in N (1s) XPS studies of nitrogen-containing organic molecules. Appl Surf Sci 45:221–227
51. Pippig F, Sarghini S, Holländer A, Paulussen S, Terryn H (2009) TFAA chemical derivatization and XPS. Analysis of OH and NH_x polymers. Surf Interface Anal 41:421–429
52. Mendes P, Belloni M, Ashworth M, Hardy C, Nikitin K, Fitzmaurice D, Critchley K, Evans S, Preece J (2003) A novel example of X-ray-radiation-induced chemical reduction of an aromatic nitro-group-containing thin film on SiO_2 to an aromatic amine film. ChemPhysChem 4:884–889
53. CSID:9161383 (2018) ChemSpider, RSC. http://www.chemspider.com/Chemical-Structure.9161383.html. Accessed 5 July 2018